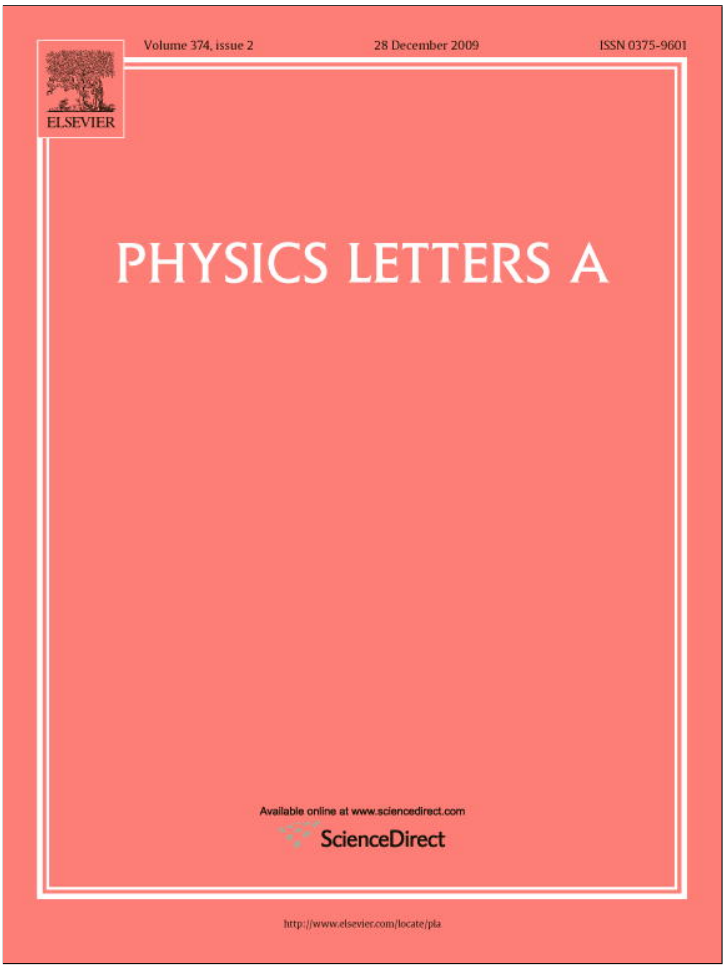

Physics Letters A 374 (2009) 191–201

Contents lists available at ScienceDirect

Physics Letters A

www.elsevier.com/locate/pla

Bifurcations of the normal modes of the Ne···Br_2 complex

Fernando Blesa [a], Jorge Mahecha [b], J. Pablo Salas [c], Manuel Iñarrea [c,*]

[a] Departamento de Física Aplicada, Universidad de Zaragoza, Zaragoza, Spain
[b] Instituto de Física, Universidad de Antioquia, Medellín, Colombia
[c] Área de Física Aplicada, Universidad de La Rioja, Logroño, Spain

ARTICLE INFO

Article history:
Received 23 June 2009
Received in revised form 14 September 2009
Accepted 16 October 2009
Available online 24 October 2009
Communicated by A.P. Fordy

PACS:
05.45.-a
45.20.Jj
34.10.+x
31.15.xv

ABSTRACT

We study the classical dynamics of the rare gas-dihalogen Ne···Br_2 complex in its ground electronic state. By considering the dihalogen bond frozen at its equilibrium distance, the system has two degrees of freedom and its potential energy surface presents linear and T-shape isomers. We find the nonlinear normal modes of both isomers that determine the phase space structure of the system. By means of surfaces of section and applying the numerical continuation of families of periodic orbits, we detect and identify the different bifurcations suffered by the normal modes as a function of the system energy. Finally, using the Orthogonal Fast Lyapunov Indicator (OFLI), we study the evolution of the fraction of the phase space volume occupied by regular motions.

1. Introduction

It is well known that nonlinear classical and semiclassical mechanics have proven to be very useful for interpreting the quantum dynamics of real atomic and molecular systems, even when the classical dynamics is chaotic and the quantum dynamics is strongly mixed [1]. Due to the simplicity of the model, the hydrogen atom in the presence of external fields is the keystone system on which all nonlinear classical tools have been successfully applied [2]. In particular, the studies of the periodic orbits and the corresponding phase space structure provide a very useful information that can be compared with the behavior of the corresponding quantum system and with the experiments [1,3]. Since the pioneering work of Gutzwiller [4], many authors (see, e.g., Ref. [5] and references therein) have stated a clear relation between classical periodic orbits and quantum eigenfunctions.

In relation to molecules, and in spite of the difficulties of dealing with in general more complex systems, a wide variety of molecular systems have been studied by using periodic orbit theory. In this sense, among a plethora of works, we refer the reader to those of Efstathiou and Contopoulos [6], Farantos [7] and Ezra [8].

A nice example where classical dynamics is playing an important role are the rare gas-dihalogen van der Walls molecules. These molecules are simple systems where several phenomena can be studied by combining classical and quantal studies. In particular, much effort has been paid to the study of the vibrational predissociation [9,10] and photodissociation [11] of these molecules. In these processes, nonlinear dynamics is particularly useful to understand the decay of the complex due to the energy transfer from the dihalogen bond to the weak van der Waals bond. However, not much attention has been paid to the vibrational dynamics of the rare gas around the dihalogen dimer. With this kind of study, widely applied in the LiCN and HCP molecules [12], it is possible to determine the structure of the phase space. As it is well known, periodic orbits are the backbone of the phase space. Moreover, they play an important role because they are essential to understand some quantum features as the localization of quantum states along unstable periodic orbits [13].

With this in mind, here we focus on the evolution of the phase space structure of one of these rare gas-dihalogen complexes: the Ne···Br_2 complex in the ground electronic state. This study is based on a systematic searching of periodic orbits by using numerical continuation of families of periodic orbits. The Letter is organized as follows. In Section 2 we describe the potential energy surface and the Hamiltonian we used in the study. We find the basic periodic orbits (normal modes) that determine the fundamental phase space structure in Section 3. In Section 4 we detect and classify by numerical continuation the different bifurcations that determine the evolution of the phase space. In Section 5 we study the evolution of the fraction of the phase space volume occupied by regular motions as a function of the energy. Finally, in Section 6 the main results are summarized.

* Corresponding author.
E-mail address: manuel.inarrea@unirioja.es (M. Iñarrea).

0375-9601/$ – see front matter
doi:10.1016/j.physleta.2009.10.050

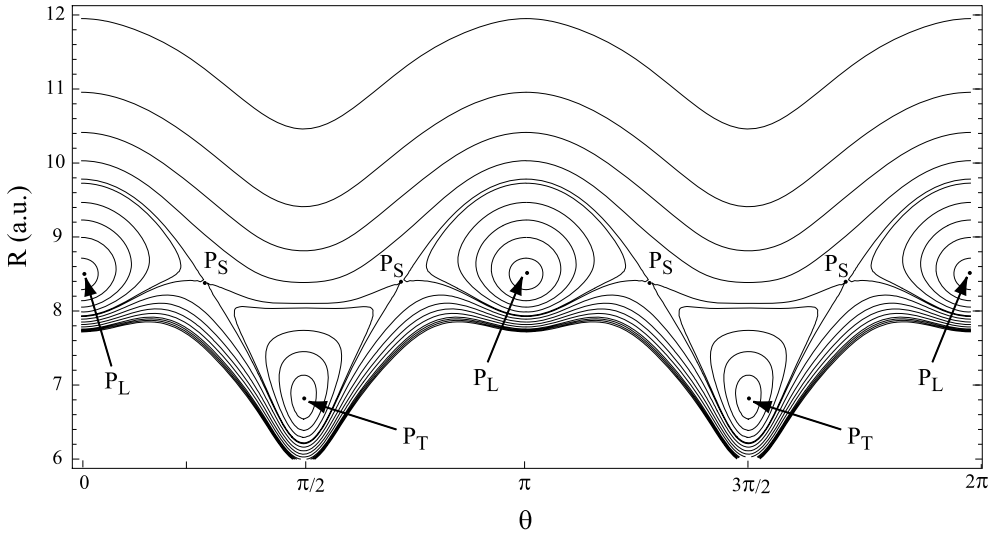

Fig. 1. Equipotential curves of the potential energy surface $V(R,\theta,r_e)$.

2. The Hamiltonian

We consider the motion of a Ne atom around a Br_2 molecule which bond coordinate r is frozen at its equilibrium distance $r_e \approx 2.281$ Å. By considering that the total angular momentum of the molecule is zero, the dynamics of the Ne atom around the Br_2 dimer is described by the two-dimensional Hamiltonian [14]

$$\mathcal{H} = \frac{P_R^2}{2\mu_2} + \frac{1}{2}\left(\frac{1}{\mu_2 R^2} + \frac{1}{\mu_1 r_e^2}\right)P_\theta^2 + V(R,\theta,r_e). \tag{1}$$

In Hamiltonian (1), R is the distance of the Ne atom to the Br–Br center of mass, θ is the angle between R and r_e, (P_R, P_θ) are the canonical momenta conjugated of R and θ and $\mu_1^{-1} = m_{\mathrm{Br}}^{-1} + m_{\mathrm{Br}}^{-1}$ and $\mu_2^{-1} = m_{\mathrm{Ne}}^{-1} + (2m_{\mathrm{Br}})^{-1}$ are the diatomic and triatomic reduced masses. Finally, $V(R,\theta,r_e)$ is the potential energy surface describing the interaction of the Ne atom with the Br_2 molecule. Throughout the Letter atomic units are used.

In order to perform classical calculations, an analytical potential energy surface (PES) is the most suitable choice. We built the PES from the *ab initio* data calculated in [10]. Using these data and following the collocation procedure also reported in Ref. [10], an expansion in Legendre polynomials $P_\lambda(\cos\theta)$ allows one to write the PES as

$$\begin{aligned} V(R,\theta,r_e) &= \sum_\lambda \left\{ \sum_{i=1}^{5} \alpha_{i\lambda}\left[e^{-2\beta_i(R-\gamma_i)} - 2e^{-\beta_i(R-\gamma_i)}\right] - \frac{\delta_\lambda}{R^6} - \frac{\eta_\lambda}{R^8} \right\} \\ &\quad \times P_\lambda(\cos\theta), \quad \lambda = 0,2,4,6,8, \end{aligned} \tag{2}$$

where the parameters are listed in Table II of Ref. [10]. Note that as for $\lambda = 0,2,4,6,8$ the Legendre polynomials are periodic functions of period π, the potential energy surface $V(R,\theta,r_e)$ and the Hamiltonian $\mathcal{H}$ are also periodic functions of the same period in the θ angle.

In Fig. 1 the equipotential curves of (2) are shown. At $R = 8.479433$ a.u. and $\theta = 0$ and $\theta = \pi$ the PES has two equivalent minima P_L of energy $E_L = -0.000427$ a.u. These minima correspond to the linear isomer of the molecule. At $R = 6.798360$ a.u. and $\theta = \pi/2$ and $\theta = 3\pi/2$ the potential energy surface $V(R,\theta,r_e)$ presents two additional minima P_T of $E_T = -0.000388$ a.u. which correspond to the so-called T-shape isomer. The linear and T-shape potential wells are kept apart by a separatrix passing through four saddle points P_S of energy $E_S = -0.000219$ a.u. located at $R = 8.383587$ a.u. and $\theta = 0.876222$, $\theta = 2.265371$, $\theta = 4.017815$ and $\theta = 5.406964$.

From the shape of $V(R,\theta,r_e)$ we deduce that the Ne atom can move in different regions of motion. There is one region of rotational orbits for energies above the isomerization barrier E_S and four regions of vibrational orbits for energies below E_S. When the energy E of the atom is below E_S, the atom is in a vibrational mode because it is always confined inside one of the four potential wells. In other words, the Ne atom is mainly aligned along the linear or the T-shape configurations and cannot reach large values of R. When in a rotational mode (energy bigger than the isomerization barrier E_S), the atom can travel from one potential well to other and, depending on the energy and initial conditions, can reach large values of R.

The Hamiltonian equations of motion read

$$\begin{aligned} \dot\theta &= \left(\frac{1}{\mu_2 R^2} + \frac{1}{\mu_1 r_e^2}\right)P_\theta, \\ \dot P_\theta &= -\frac{\partial V(R,\theta,r_e)}{\partial\theta}, \\ \dot R &= \frac{P_R}{\mu_2}, \\ \dot P_R &= \frac{P_\theta^2}{\mu_2 R^3} - \frac{\partial V(R,\theta,r_e)}{\partial R}. \end{aligned} \tag{3}$$

The equilibrium points of the above Hamiltonian flow are the critical points of the PES $V(R,\theta,r_e)$ together with the conditions $P_R = P_\theta = 0$. Moreover, if we consider initial conditions $P_\theta = 0$ and $\theta = 0$, $\pi/2$, π or $3\pi/2$ it is straightforward to see that in the above equations we obtain $\dot\theta = \dot P_\theta = 0$, which corresponds to pure analytic vibrational rectilinear periodic orbits passing through each of the critical points P_L and P_T of $V(R,\theta,r_e)$. We name these rectilinear orbits as L_1 and T_1, respectively.

3. Phase space structure

The computation of Poincaré surfaces of section is a common way to illustrate the structure and evolution of the phase space of a two-degrees Hamiltonian dynamical system. The construction of a surface of section is a delicate task because it should be transverse to the flow [15]. In our problem a good choice is to define the surfaces of section as the intersection of the phase trajectories with the (θ, P_θ) plane for $P_R = 0$. We choose this surface of

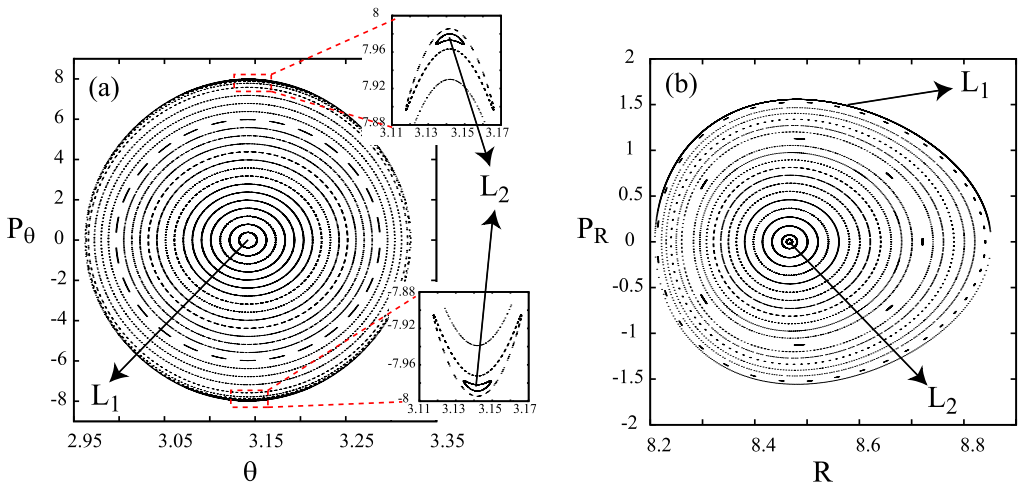

Fig. 2. (a) Poincaré surfaces of section for $P_R = 0$ and (b) for $\theta = \pi$ in the linear configuration. Both surfaces of section are calculated for the same energy $E = -0.00039$ a.u.

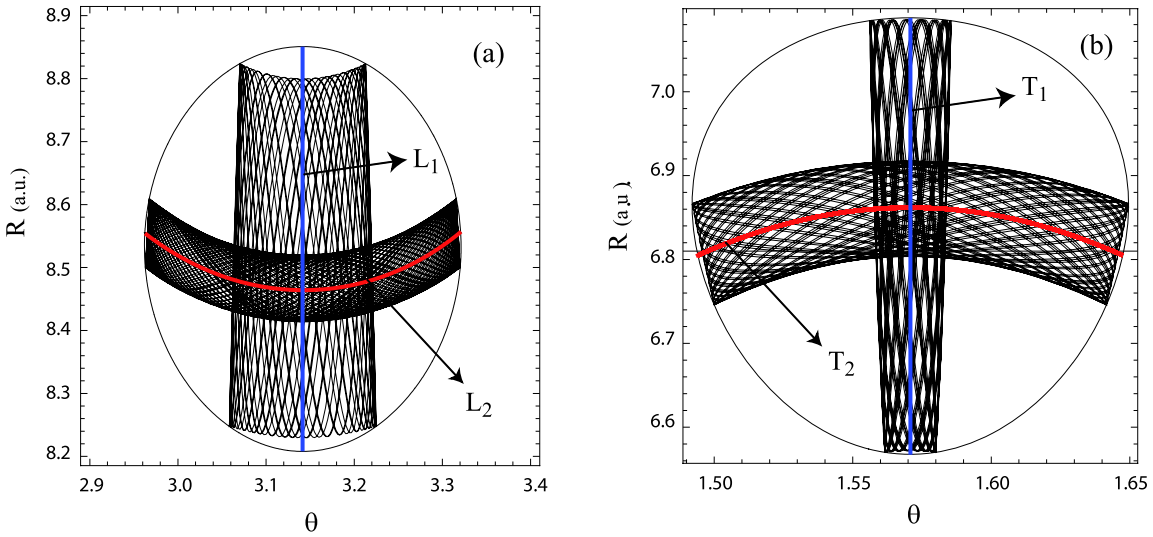

Fig. 3. The blue and red colored lines are, respectively, the rectilinear normal modes L_1 and T_1 and the angular normal modes L_2 and T_2. Examples of quasiperiodic orbits around these periodic orbits are also shown. Figures have been calculated for energies $E = -0.00039$ a.u. (a), and $E = -0.00037$ a.u. (b). (For interpretation of the colours in this figure, the reader is referred to the web version of this Letter.)

section because all the orbits (both rotational and vibrational) will cross it at any time, e.g., we can guarantee that this surface of section is transverse to the Hamiltonian flux.

The surface of section is generated by numerical integration of the Hamiltonian equations of motion (3). These equations are solved by means of an explicit eight order Runge–Kutta algorithm with stepsize control and dense output [16].

Under the conditions of this surface of section and taking into account the Hamiltonian (1), the available region in the plane (θ, P_θ) of the surface of section is determined by the possible values of the momentum P_θ that are given by the equation

$$P_\theta = \pm\sqrt{2\frac{\mu_2\mu_1 r_e^2 R^2}{\mu_2 R^2 + \mu_1 r_e^2}\big[E - V(R,\theta,r_e)\big]}. \tag{4}$$

In Fig. 2a we show the surface of section for an energy $E = -0.00039$ a.u. This energy is above the energy E_L of the linear minimum P_L and below the energy E_T of the T-shape minima P_T. Due to the symmetry of the Hamiltonian, the complete surface of section for this energy presents two equal disjoint regions around $\theta = 0$ and $\theta = \pi$ that correspond to "trapped" motions inside each of the two potential wells of the linear isomer (for simplicity we only show in Fig. 2a the region around $\theta = \pi$). In this surface of section all the orbits are ordered defining invariant closed curves around two stable fixed points (periodic orbits) located at $(0, 0)$ and $(\pi, 0)$ respectively. These fixed points correspond to the vibrational rectilinear orbits L_1 (see Fig. 3a). In Fig. 2a is also shown a zoom of the upper and lower parts of the surface of section. In these zooms there appear two more stable fixed points which correspond to the same arch-like periodic orbit named as L_2 (see Fig. 3a). A complementary vision of the phase space structure is given by computing the surface of section $\theta = \pi$ in the (R, P_R) plane. In this case, the limit of the available region in the (R, P_R) plane is given by the equation

$$P_R = \pm\sqrt{2\mu_2\big[E - V(R,\pi,r_e)\big]}. \tag{5}$$

It is worth noting that the rectilinear orbit L_1 is tangent to the flux in this Poincaré map and it corresponds to the curves (5). When this surface of section is computed for the same value of E (see Fig. 2b) we observe a similar phase space structure as in Fig. 2a, being the central fixed point the periodic orbit L_2.

From the phase plots of Fig. 2, we deduce that the phase space in the linear potential energy well is organized around the periodic orbits L_1 and L_2. Then, the nearer a quasiperiodic orbit is to L_1 the greater its orientation is along this periodic orbit. On the other

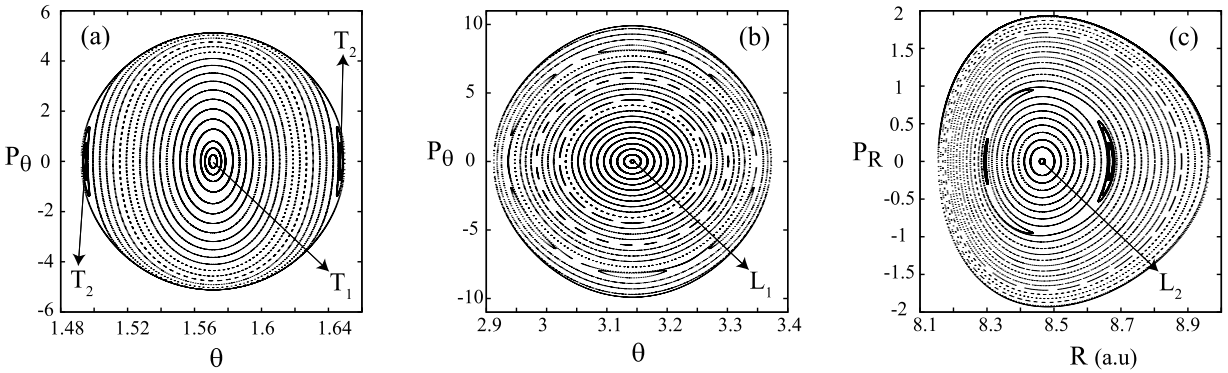

Fig. 4. (a) and (b) are, respectively, the surfaces of section for $P_R = 0$ of the T-shape $\theta = \pi/2$ isomer and the linear $\theta = \pi$ isomer. The figure (c) is the surface of section for $\theta = \pi$ of the same linear isomer. All the surfaces of section are calculated for the same energy $E = -0.00037$ a.u.

hand, the quasiperiodic orbits near L_2 show an arch-like shape. In Fig. 3a examples of these two kind of motions are shown.

In fact, it is worth noting that the periodic orbits L_1 and L_2 are, respectively, the radial and the angular nonlinear normal modes of the linear isomer.

When the energy E is above E_T and below E_S, the Ne atom can live trapped inside any of the four potential wells of $V(R, \theta, r_e)$. In this energy interval, surfaces of section will show four disjoint regions of motion. The surfaces of section in Fig. 4 correspond to an energy value $E = -0.00037$ a.u. slightly above E_T. For this energy, the linear and the T-shape phase space regions show regular motion. For simplicity we only show the surfaces of section of the T-shape $\theta = \pi/2$ isomer (Fig. 4a) and the linear $\theta = \pi$ isomer (Fig. 4b–c). The dynamics in the T-shape isomer regions (Fig. 4a) is organized around three fixed stable points located at the θ axis which are the nonlinear normal modes of the T-shape isomer. Indeed, the central fixed point is the vibrational rectilinear orbit T_1 while the other two stable fixed points correspond to the same periodic orbit. This periodic, named as T_2, is again an arch-like periodic orbit. In Fig. 3b are depicted the periodic orbits T_1 and T_2 as well as two representative quasiperiodic orbits.

In the linear isomer regions, Fig. 4b–c shows that, besides the appearance of two islands of resonances, the phase space shows a similar structure as in Fig. 2.

4. Evolution of the nonlinear normal modes

From the above study we have determined the four normal modes of the system. These normal modes are the fundamental families of periodic orbits of the system because their numerical continuation generated by the variations of the energy E and the computation of the stability parameter of each family will help us in understanding the dynamics of the problem.

As it is well known, the linear stability of a periodic orbit is determined from the eigenvalues of the monodromy matrix. Since we are dealing with a Hamiltonian problem, the eigenvalues appear in reciprocal pairs, and as a consequence of the invariance of the Hamiltonian equations of motion we have one trivial eigenvalue $\lambda_0 = 1$ with multiplicity 2. Then, the stability index

$$k = \lambda + 1/\lambda \tag{6}$$

is normally used [17], where the condition k real and $|k| < 2$ applies for linear stability, and the critical values $k = \pm 2$ mean that a new family of periodic orbits has likely bifurcated from the original one. Therefore, stability diagrams where the stability index is presented versus the parameter generator of the family are commonly used.

At this point, we proceed as follows. By using the numerical software AUTO [18] we carry out the numerical continuation of the families of the four normal modes that emanate from these solutions. The stability diagram of every periodic orbit of each family as a function of the energy E is also computed. From this diagram, we can detect values of the energy for which possible bifurcations take place. Bifurcations produce qualitative changes in the phase space structure. In the present study, when a bifurcation is found, we calculated the surfaces of section when energy is slightly less and slightly larger than its value at bifurcation, in order to illustrate the effect of bifurcation.

4.1. Linear configuration

We begin considering the linear isomer and its angular nonlinear normal mode. The diagram in Fig. 5 shows the evolution of the stability index of the family of the periodic orbits corresponding to this normal mode. This diagram gives the stability parameter k of this family in the interval -4×10^{-4} a.u. $\leqslant E \leqslant -1.2 \times 10^{-4}$ a.u. We call this family with the same name as the corresponding periodic orbit L_2. The evolution of this family is depicted in blue in Fig. 5. As it can be seen in the figure, this family L_2 suffers four different bifurcations, and it is always stable until the last bifurcation which takes place at $E \approx -1.9 \times 10^{-4}$ a.u. The first bifurcation occurs for $E \approx -3.86 \times 10^{-4}$ a.u. when the stability index reaches the critical value $k = 2$ in a tangential way (without crossing it). This is a double pitchfork bifurcation [19] in which four new periodic families (two stable ones and two unstable ones) emanate from the L_2 family. The two new stable families have the same stability index values, and thus, both branches are represented in Fig. 5 by the same continuous red line. The same occurs with the two new unstable families (dashed red line).

This bifurcation is visualized in Fig. 6 by means of surfaces of section for $\theta = \pi$. In Fig. 6a, when $E = -3.9 \times 10^{-4}$ a.u., the SOS only exhibits one fixed center point corresponding to the angular normal mode L_2. This periodic motion is depicted in blue in the (θ, R) plane in Fig. 6c–d. After the bifurcation, for $E = -3.82 \times 10^{-4}$ a.u., two new center points and two saddle points arise in the SOS emanating from L_2, see Fig. 6b. The two new stable periodic motions are drawn in red in the (θ, R) plane in Fig. 6d. The orbits of both motions have the same shape in this plane but they are traveled in opposite directions.

The second bifurcation takes place for $E \approx -3.08 \times 10^{-4}$ a.u. when the stability index reaches the critical value $k = -2$. This is a double period-doubling bifurcation [19] in which four new periodic families (two stable ones and two unstable ones) emerge from the normal mode L_2. All these new periodic orbits have double period of L_2 and, therefore have a periodicity $m = 2$ [19]. The two new stable families have the same stability index values, and therefore, both branches are represented in Fig. 5 by the same continuous clear green line. The same happens with the two new un-

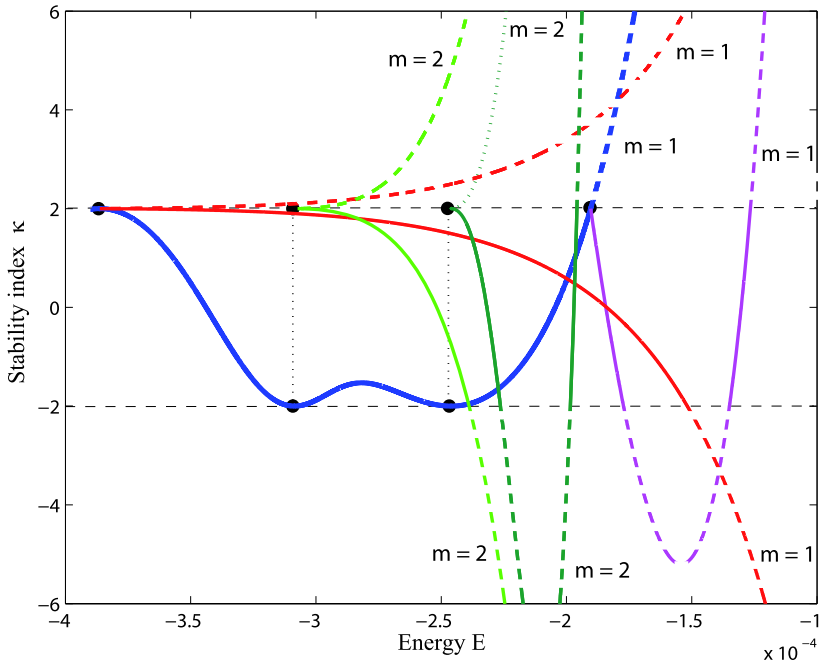

Fig. 5. Stability diagram of the families of the periodic orbits emanating from the angular nonlinear normal mode of the linear isomer as a function of the energy E. Dashed lines stand for unstable periodic orbits. (For interpretation of the colours in this figure, the reader is referred to the web version of this Letter.)

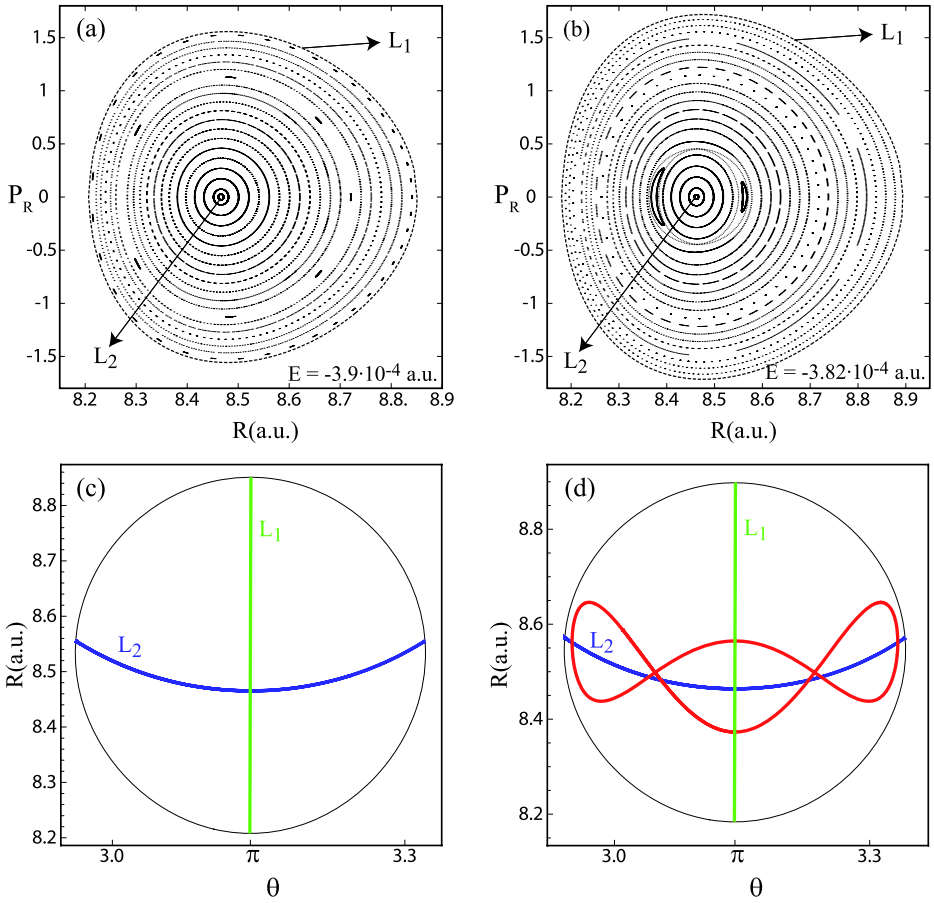

Fig. 6. First bifurcation of the angular nonlinear normal mode family in the linear isomer. Surfaces of section for $\theta = \pi$ before (a) and after (b) the double pitchfork bifurcation. Stable periodic orbits before (c) and after (d) bifurcation. Red line represents the new stable periodic orbits arisen from the bifurcation. (For interpretation of the colours in this figure, the reader is referred to the web version of this Letter.)

stable families (dashed clear green lines). Fig. 7 represents the evolution of the surface of section $\theta = \pi$ through this bifurcation, as well as the stable periodic motions involved in it. The orbit in the (θ, R) plane of this periodic motion is shown in blue in Fig. 7c–d.

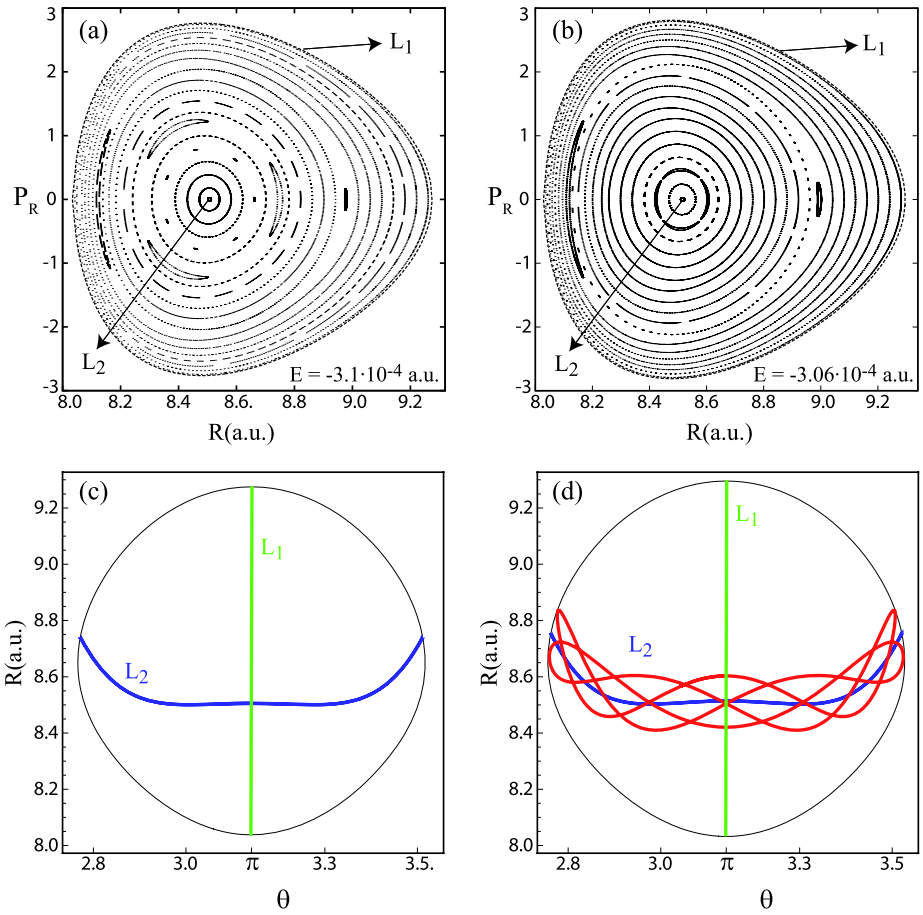

Fig. 7. Second bifurcation of the angular nonlinear normal mode family in the linear isomer. Surfaces of section for $\theta = \pi$ before (a) and after (b) the double period-doubling bifurcation. Stable periodic orbits before (c) and after (d) bifurcation. Red line represents the new stable periodic orbits arisen from the bifurcation. (For interpretation of the colours in this figure, the reader is referred to the web version of this Letter.)

After bifurcation occurs, see Fig. 7b for $E = -3.06 \times 10^{-4}$ a.u., four new center points and four new saddle points appear in the SOS emerged form L_2. Each pair of the four new center points corresponds to each one of the two new stable periodic motions. Fig. 7d shows as a red line the orbit of these two new stable motions plotted in the (θ, R) plane. The orbit shape of these two motions are the same, but they are traveled in opposite directions.

The third bifurcation occurs for $E \approx -2.46 \times 10^{-4}$ a.u., it is also a double period-doubling one and, thus it is very similar to the previous bifurcation. Two new stable periodic families and two new unstable ones arise from the angular normal mode L_2, see Fig. 5. All these new families have twice the period of L_2, that is, they have multiplicity $m = 2$. As it can be seen in Fig. 8a–b, the surfaces of section $\theta = \pi$ show that a region of chaotic motions surrounding these periodic motion has already appeared for this energy range. This chaotic region increases quickly after the bifurcation. The orbit of the angular normal mode L_2 has taken a W-like shape in the (θ, R) plane for this energy, see the blue line in Fig. 8c–d. The orbits of the two new stable periodic motions emerged from this bifurcation are shown as red and orange lines in Fig. 8d. It is important to note that, unlike all the previous stable periodic motions, the shapes of these new ones are not symmetric with respect to the $\theta = \pi$ axis in the (θ, R) plane, but they are as mirror reflections one each other.

The last bifurcation in the angular normal mode L_2 of the linear isomer takes place for $E \approx -1.9 \times 10^{-4}$ a.u., when the stability index crosses the critical value $k = 2$, see Fig. 5. This is a pitchfork bifurcation in which the angular mode L_2 changes its stability becoming an unstable periodic motion ($k > 2$). At the same time, two new periodic stable motions with the same period of L_2 arise from it. For this energy range, Fig. 9a–b shows that most of the surface of section is filled by chaotic motions. The center fixed point corresponding to L_2 before bifurcation, transforms after it into a saddle point and two nearby center points corresponding to the two new stable periodic motions. The orbits of these two new stable motions plotted in the (θ, R) plane are shown as red and orange lines in Fig. 9d. As it happens in the previous bifurcation, the shapes of these new periodic motions are not symmetric with respect to the $\theta = \pi$ axis in the (θ, R) plane, but they are as mirror reflections one each other. As this energy range is above the isomerization energy barrier E_S, the equipotential curves of Fig. 9c–d are not closed because the potential wells of both isomers are connected in these situations. Nevertheless, the periodic motions involved in this bifurcation are confined in the potential well of the linear isomer.

On the other hand, the radial nonlinear normal mode of the linear isomer follows a much simpler evolution with the energy. Fig. 10a shows the stability diagram of the family of the periodic orbits corresponding to this normal mode. This diagram gives the stability parameter k of this family in the interval -4×10^{-4} a.u. $\leqslant E \leqslant -0.5 \times 10^{-4}$ a.u. We call this family with the same name as the corresponding periodic orbit L_1. The evolution of this family is depicted in blue in Fig. 10a. This family L_1 only suffers one bifurcation, as it can be seen in that figure. This bifurcation occurs for $E \approx -2.16 \times 10^{-4}$ a.u., when the stability index crosses the critical value $k = -2$. This is a period-doubling bifurcation in which the normal mode L_1 changes its stability becoming unstable,

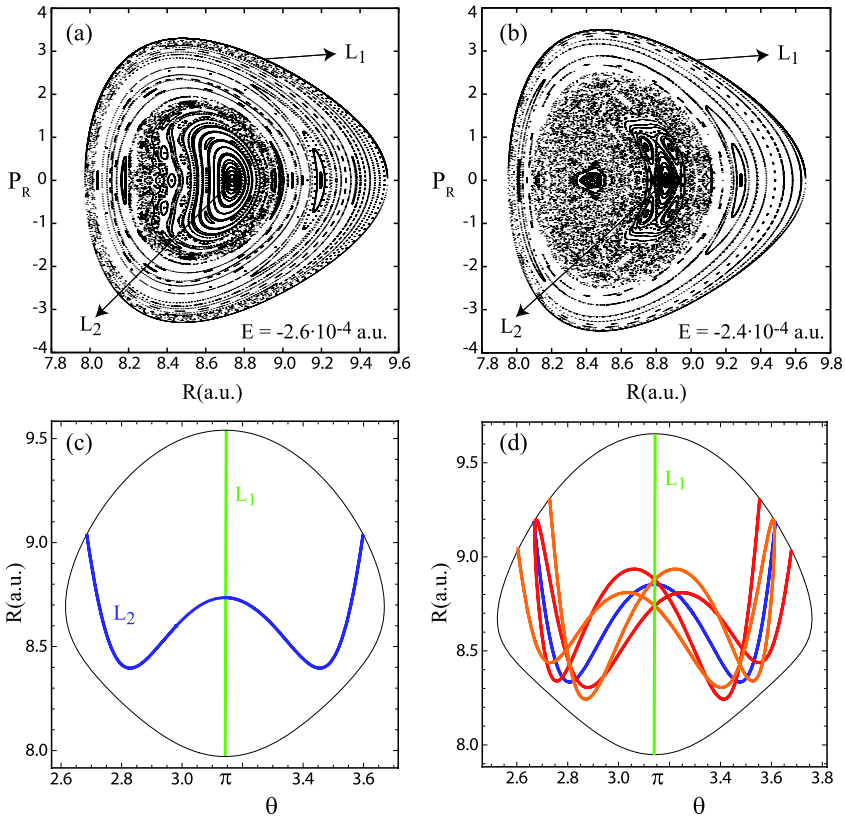

Fig. 8. Third bifurcation of the angular nonlinear normal mode family in the linear isomer. Surfaces of section for $\theta = \pi$ before (a) and after (b) the double period-doubling bifurcation. Stable periodic orbits before (c) and after (d) bifurcation. Red and orange lines represent the two new stable periodic orbits arisen from the bifurcation. (For interpretation of the colours in this figure, the reader is referred to the web version of this Letter.)

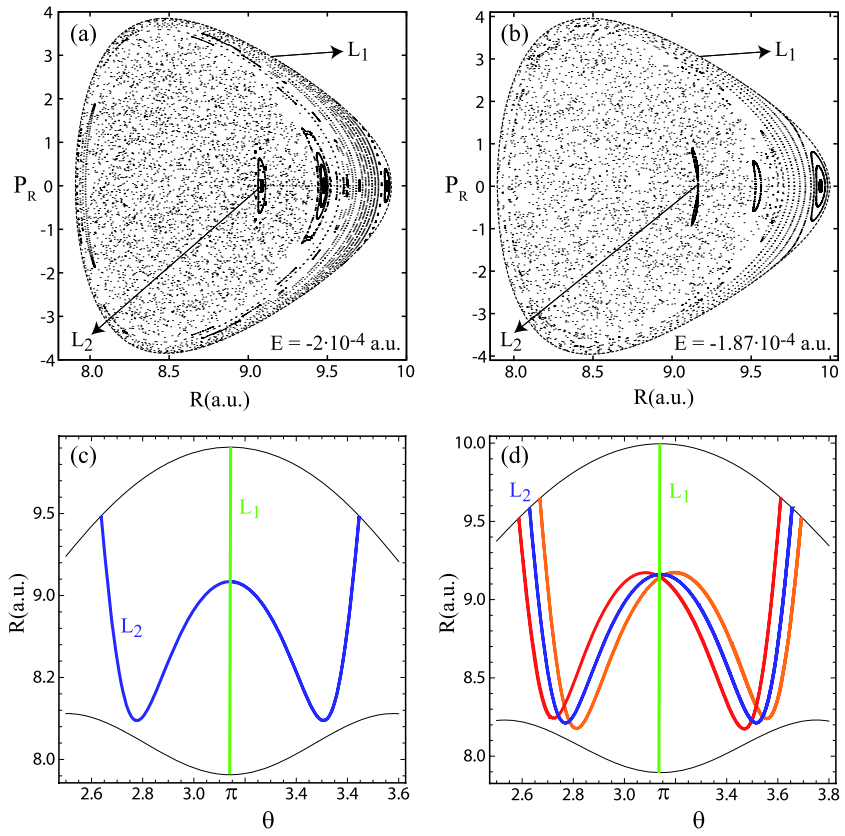

Fig. 9. Fourth bifurcation of the angular nonlinear normal mode family in the linear isomer. Surfaces of section for $\theta = \pi$ before (a) and after (b) the pitchfork bifurcation. Periodic orbits before (c) and after (d) bifurcation. Red and orange lines represent the two new stable periodic orbits arisen from the bifurcation. (For interpretation of the colours in this figure, the reader is referred to the web version of this Letter.)

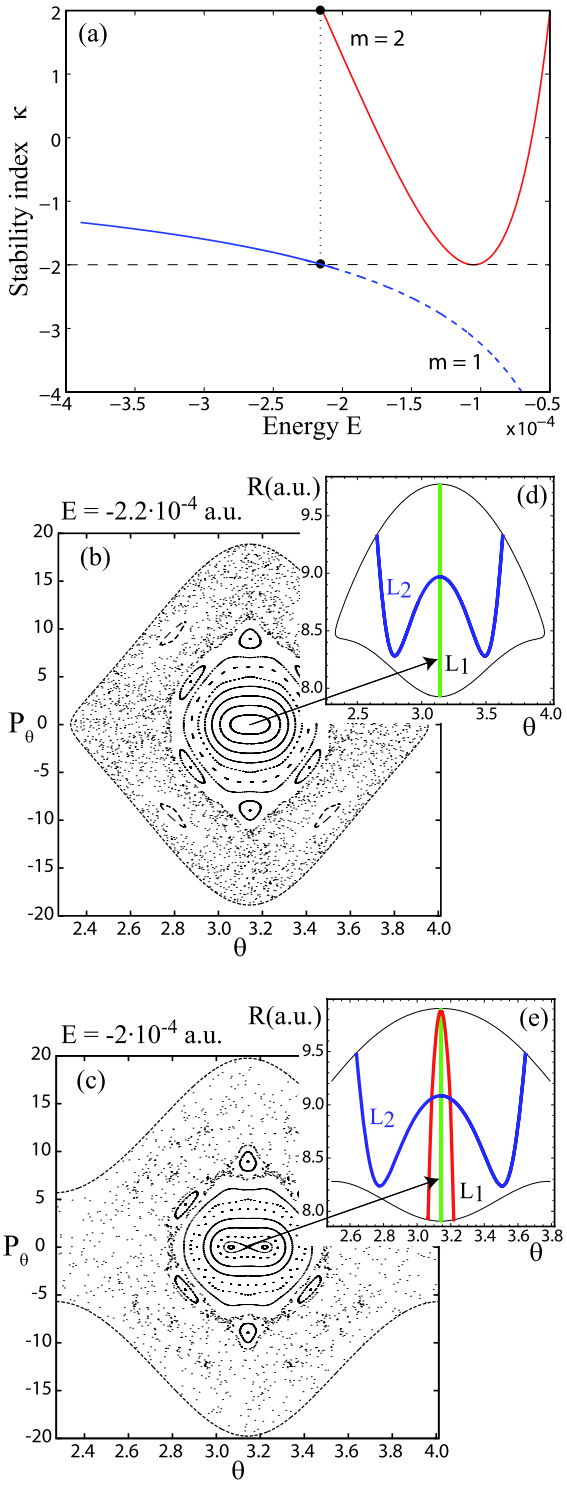

Fig. 10. Bifurcation of the radial nonlinear normal mode family in the linear isomer. (a) Stability diagram of the family of the periodic orbits as a function of the energy E. Surfaces of section for $P_R = 0$ before (b) and after (c) the period-doubling bifurcation. Periodic orbits before (d) and after (e) bifurcation. Red line represents the new stable periodic orbit arisen from the bifurcation. (For interpretation of the colours in this figure, the reader is referred to the web version of this Letter.)

and simultaneously a new periodic stable motion emerges from L_1, represented as a red line in Fig. 10a. This new stable motion has twice the period of L_1, and thus a multiplicity $m = 2$.

In order to visualize this bifurcation in a clearer way, we have made use of surfaces of section for $P_R = 0$ instead of the previous one $\theta = \pi$, because in the last one, the radial normal mode L_1 appears as the limit of the SOS. Fig. 10b–c shows the SOS $P_R = 0$ before (b) and after (c) the bifurcation takes place. In these figures it can be seen how the fixed center point corresponding to L_1 becomes a saddle point and two new center points along the $P_\theta = 0$ axis. These two new center points correspond to the new stable periodic motion of multiplicity $m = 2$. For this energy range, great part of the SOS is covered by chaotic motions. Fig. 10d–e shows as a green line the orbit of the radial mode L_1 plotted in the (θ, R) plane, as well as the orbit of the new stable periodic motion (red line) arisen from the bifurcation. As the energy considered after the bifurcation, $E = -2 \times 10^{-4}$ a.u., is above the isomerization energy barrier E_S, the SOS of Fig. 10c and the equipotential curve of Fig. 10e are not closed because in that case, the potential wells of both isomers are connected. However, the periodic motions involved in this bifurcation remain confined in the well of the linear configuration. Moreover, around the periodic orbits involved in this bifurcations there exist islands of regular motion confined in the well of the linear configuration.

4.2. T-shape configuration

With regards to the T-shape isomer, we also begin considering the angular nonlinear normal mode. Fig. 11a shows the stability diagram of the family of the periodic orbits corresponding to this normal mode. This diagram gives the stability parameter k of this family in the interval -3.8×10^{-4} a.u. $\leqslant E \leqslant -2.2 \times 10^{-4}$ a.u. We call this family with the same name as the corresponding periodic orbit T_2. As it can be seen in this figure, the evolution of the T_2 family with the energy, represented by a blue line, is only affected by a bifurcation, that takes place for $E \approx -2.75 \times 10^{-4}$ a.u., when the stability index crosses the critical value $k = 2$. This is a pitchfork bifurcation in which the normal mode T_2 changes its stability becoming unstable, and simultaneously two new periodic stable motions emerge from T_2. Both new stable periodic motions have the same stability index values, and thus, they are represented with the same red line in Fig. 11a.

As we are considering now the T-shape configuration whose potential well is centered at $\theta = \pi/2$, this bifurcation is better visualized in Fig. 11b–c making use of surfaces of section for $\theta = \pi/2$. The angular normal mode T_2, that appears before the bifurcation as a fixed center point located at the $P_R = 0$ axis (Fig. 11b), transforms after bifurcation into a saddle point and two new center points situated symmetrically with respect to the $P_R = 0$ axis (Fig. 11c). Each one of these new center points corresponds to one of the two new stable periodic motions emerged from this bifurcation. As it also can be seen in these figures, most of the SOS is filled by chaotic motions for this energy range. It is important to note that in the T-shape configurations chaotic motions appear more quickly than in the linear one. In Fig. 11d–e the orbit of the normal mode T_2 is plotted in the (θ, R) plane as a blue line. The orbits of the two new stable periodic motions are also represented by red and orange lines in Fig. 11e. It is interesting to note that, unlike the normal mode T_2, the shapes of these new periodic motions are not symmetric with respect to the $\theta = \pi/2$ axis, but they are as mirror reflections one each other.

On the other hand, Fig. 12a shows the stability diagram in the interval -4×10^{-4} a.u. $\leqslant E \leqslant -1.5 \times 10^{-4}$ a.u. of the family of the periodic orbits T_1 corresponding to the radial nonlinear normal mode of the T-shape isomer. The evolution of this family with the energy, that is represented in this figure by the blue line, is only affected by a bifurcation for $E \approx -2.65 \times 10^{-4}$ a.u., when the stability index crosses the critical value $k = -2$. This is a period-doubling bifurcation in which the radial normal mode T_1 changes its stability becoming unstable, and at the same time a new periodic stable motion emerges from T_1. This new stable family,

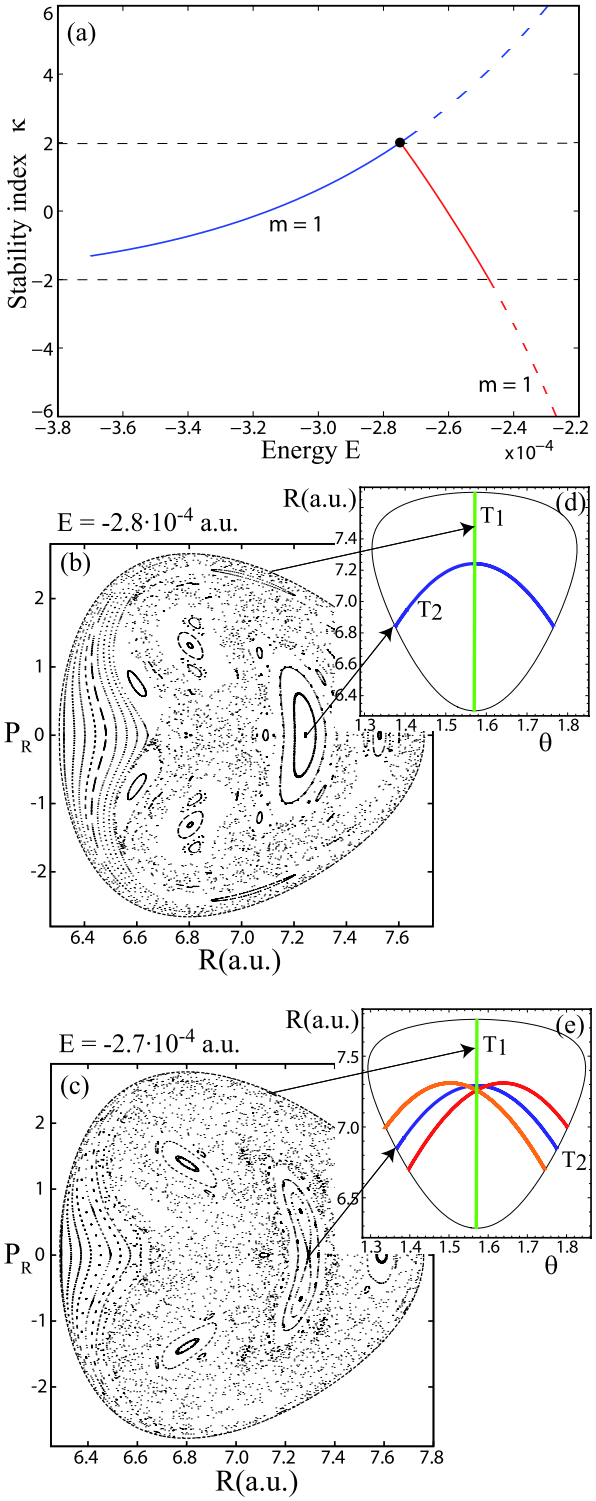

Fig. 11. Bifurcation of the angular nonlinear normal mode family in the T-shape isomer. (a) Stability diagram of the family of the periodic orbits as a function of the energy E. Surfaces of section for $\theta = \pi/2$ before (b) and after (c) the pitchfork bifurcation. Periodic orbits before (d) and after (e) bifurcation. Red and orange lines represent the two new stable periodic orbits arisen from the bifurcation. (For interpretation of the colours in this figure, the reader is referred to the web version of this Letter.)

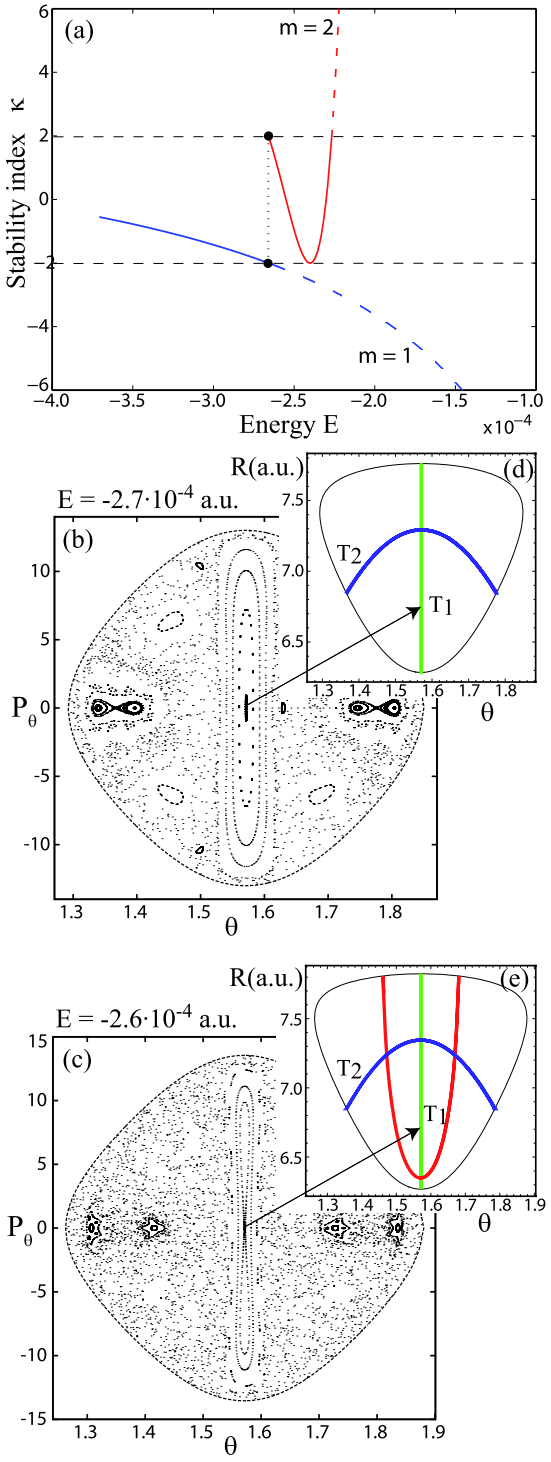

Fig. 12. Bifurcation of the radial nonlinear normal mode family in the T-shape isomer. (a) Stability diagram of the family of the periodic orbits as a function of the energy E. Surfaces of section for $P_R = 0$ before (b) and after (c) the period-doubling bifurcation. Periodic orbits before (d) and after (e) bifurcation. Red line represents the new stable periodic orbit arisen from the bifurcation. (For interpretation of the colours in this figure, the reader is referred to the web version of this Letter.)

plotted as a red line in Fig. 12a, has twice the period of T_1 and a multiplicity $m = 2$.

This bifurcation is portrayed in Fig. 12b–c by means of surfaces of section for $P_R = 0$. The new center points correspond to the new stable periodic motion of multiplicity $m = 2$. For these energy values, similar to those of the previous bifurcation of the angular mode, great part of the SOS is covered by chaotic motions. Fig. 12d–e shows as a green line the orbit of the radial normal mode T_1 plotted in the (θ, R) plane, as well as the orbit of the new stable periodic motion (red line) emerged from the bifurcation.

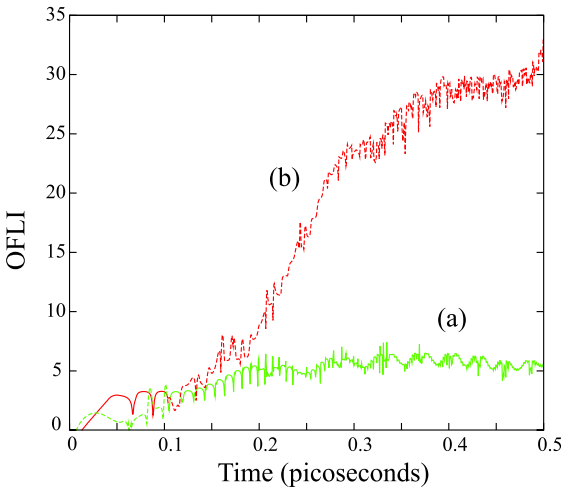

Fig. 13. Evolution of the OFLI indicator as function of time for (a) a regular trajectory and (b) a chaotic trajectory. Initial conditions of both orbits has been taken from Fig. 9b. (For interpretation of the colours in this figure, the reader is referred to the web version of this Letter.)

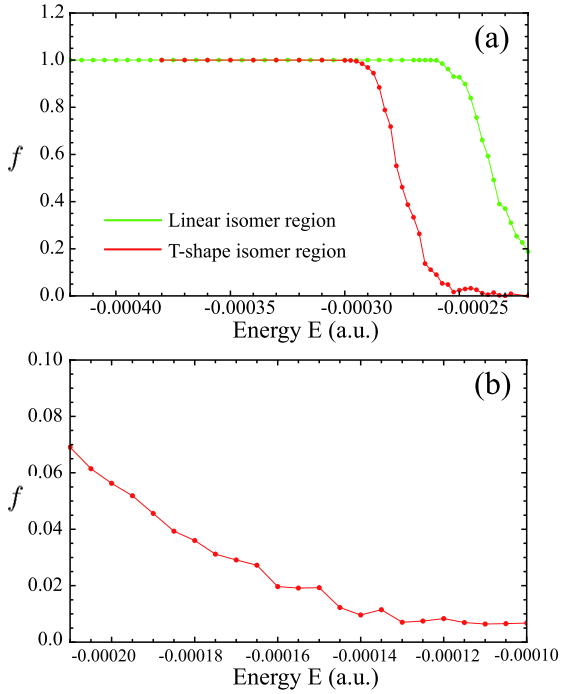

Fig. 14. (a) Fraction f of the phase space volume occupied by regular trajectories in the accessible linear (green line) and T-shape phase space volumes as a function of the energy $E < E_S$. (b) Evolution of the fraction f for energy $E > E_S$. (For interpretation of the colours in this figure, the reader is referred to the web version of this Letter.)

5. Chaotic behavior

As we observe in the gallery of surfaces of section throughout the Letter, as the energy increases, the regions of stochasticity grow in size. A clear way to illustrate this fact is to measure the fraction f of the phase space volume occupied by regular trajectories. To do this, for a given value of the energy E, we have numerically calculated the Orthogonal Fast Lyapunov Indicator (OFLI) [20] of a large number of orbits (around ten thousand) with initial conditions filling the accessible phase space volume. The OFLI indicator has been computed up to a cut-off value of 0.5 picoseconds. This time value is long enough for the system to display its regular or chaotic behavior. Fig. 13 shows the evolution of the Lyapunov indicator as a function of time for a chaotic trajectory and a regular trajectory with initial conditions taken from the surface of section of Fig. 9b. In this figure we observe that, after a short time integration, the OFLI indicator is able to distinguish between regular and chaotic trajectories.

Taking into account that when the energy of the system is below the saddle point energy E_S, the Ne atom remains confined inside the linear or the T-shape potential wells, we carry out the calculation of the fraction f in the following way. On the one side, in the energy interval $E_L < E < E_S$ we compute the fractions of regular trajectories in the linear (f_L) and in the T-shape (f_T) disjoints phase space volumes. The results of these computations are shown in Fig. 14a. On the other hand, because when $E > E_S$ the linear and the T-shape space regions are connected, we calculate a unique fraction f corresponding to this global phase space region. The result of the calculation is presented in Fig. 14b.

In Fig. 14a the evolution of f_T indicates that until energy values near $E = -0.0003$ a.u. the T-shape phase space is filled with regular orbits. From this energy value, a quick decrease of f_T takes place, in such a way that for values of E close to -0.00023 a.u. most of the phase space is chaotic ($f_T \approx 0$). We find a similar behavior in the phase space region of the linear configuration. Form energy values close to -0.00026 a.u., the fraction f_L decreases, although due to the presence of the island around the periodic orbit L_1, it remains above 0.18.

The evolution of the fraction f when the energy is bigger than E_S is shown in Fig. 14b. As the energy increases, the percentage f of regular orbits decreases, being nearly zero for energy values bigger than -0.0001 a.u.

6. Conclusions

In the present work, we have studied the classical dynamics of the rare gas-dihalogen Ne···Br_2 complex in its ground electronic state. Owing to the fact that the van der Waals bond between the Ne atom and the Br_2 dimer is much weaker than the dihalogen bond, we have considered this bond frozen at its equilibrium distance, and therefore we have treated this molecular complex as a system of two degrees of freedom. We have also restricted our study to the case in which the total angular momentum of the complex is taken to be zero.

Under these assumptions, the potential energy surface of the system has two pairs of minima: one pair corresponds to the two equivalent linear configurations of the complex, and the other pair corresponds to the T-shape configurations. These four potential wells are separated by four saddle points.

By direct inspection of the equations of motion and using suitable Poincaré surfaces of section, we have found four stable basic periodic orbits that determine the phase space structure of the system. These basic periodic motions are the nonlinear normal modes of both linear and T-shape isomers. Each one of both configurations has one radial normal mode and one angular mode. Moreover, by means of the surfaces of section and applying the numerical continuation of families of periodic orbits, we have studied the evolution the normal modes of both isomers as a function of the system energy.

We have detected and identified the different bifurcations suffered by the normal modes, as well as the new periodic orbits emanated from the bifurcations. For increasing values of the energy, the angular mode of the linear isomer undergoes a sequence of four bifurcations: a double pitchfork one, two consecutive double period-doubling ones, and at last a simple pitchfork one, in which this normal mode becomes unstable. Each one of the other normal modes only suffers one bifurcation: either a pitchfork one or a period-doubling one, in which they turn into unstable periodic motions.

Although some of the detected bifurcations take place for energy values above the isomerization energy barrier, we have found that the orbits of the normal modes and the new periodic motions involved in the bifurcations remain confined in the potential well of the corresponding isomer. On the other hand, even though the shape of the orbits of the normal modes are always symmetric with respect to the angular coordinate for all considered energy values, we have detected that in some of the bifurcations, the new arisen periodic orbits lose this kind of symmetry in their shapes.

With respect to the evolution of the phase space, for small values of energy, the phase space presents quite regular structure with quasiperiodic motions organized around the normal modes of both configurations. Nevertheless, for increasing values of the energy, the regularity of the system dynamics decrease because the phase space begins to be filled by growing regions of chaotic motions. By means of the Orthogonal Fast Lyapunov Indicator (OFLI), we have studied the evolution of the fraction of the phase space volume occupied by regular motions. In this way, we have found that the dynamics of the T-shape isomer loses its regularity much more quickly than the linear isomer dynamics. For energy values above the isomerization energy barrier the system dynamics is almost completely dominated by chaotic motions.

There are some potential directions for future studies. In particular, the extension of this study when the total angular momentum of the complex is not zero is now under consideration.

Acknowledgements

This work is included in the framework of the research projects MTM2005-08595, MTM2008-03818 and AYA2008-05572 supported by the Spanish Ministry of Education and Science. J.M. thanks the support from Programa de Sostenibilidad Universidad de Antioquia.

References

[1] S.C. Farantos, Int. Rev. Phys. Chem. 15 (1996) 345;
M. Davis, J. Chem. Phys. 107 (1997) 106.
[2] J. Main, G. Wiebusch, A. Holle, K.H. Welge, Phys. Rev. Lett. 57 (1986) 2789;
A. Holle, G. Wiebusch, K.H. Welge, Z. Phys. D: At. Mol. Clusters 6 (1987) 295;
H. Friedrich, D. Wintgen, Phys. Rep. 183 (1989) 37;
G. Raithel, M. Fauth, H. Walther, Phys. Rev. A 44 (1991) 1898;
A.D. Peters, J.B. Delos, Phys. Rev. A 47 (1993) 3020;
A.D. Peters, J.B. Delos, Phys. Rev. A 47 (1993) 3036;
J.-M. Mao, K.A. Rapelje, S.J. Blodgett-Ford, J.B. Delos, Phys. Rev. A 48 (1993) 2117.
[3] S. Keshavamurthy, G. Ezra, J. Chem. Phys. 107 (1997) 156.
[4] M.C. Gutzwiller, Chaos in Classical and Quantum Mechanics, Springer-Verlag, New York, 1990.
[5] J. Main, G. Wunner, Phys. Rev. Lett. 82 (1999) 3038.
[6] K. Efstathiou, G. Contopoulos, Chaos 11 (2001) 327.
[7] For a complete list of papers by S. Farantos, please visit his home page: http://tccc.iesl.forth.gr/farantos.
[8] For a complete list of papers by G. Ezra, please visit his home page: http://www.chem.cornell.edu/gse1/gsehome.html.
[9] A.A. Granovsky, A.V. Medvedev, A.A. Buchachenko, N.F. Stepanov, J. Chem. Phys. 108 (1998) 6282.
[10] R. Prosmiti, C. Cunha, A.A. Buchachenko, G. Delgado-Barrio, J. Chem. Phys. 117 (2002) 10019.
[11] R. Prosmiti, P. Villarreal, G. Delgado-Barrio, O. Roncero, Chem. Phys. Lett. 359 (2002) 229.
[12] F.J. Arranz, F. Borondo, R.M. Benito, J. Chem. Phys. 104 (1996) 6401;
F.J. Arranz, F. Borondo, R.M. Benito, J. Chem. Phys. 107 (1997) 2395;
J.C. Losada, J.M. Estebaranz, R.M. Benito, F. Borondo, J. Chem. Phys. 108 (1998) 63;
F.J. Arranz, R.M. Benito, F. Borondo, J. Chem. Phys. 123 (2005) 044301;
Z.S. Safi, J.C. Losada, R.M. Benito, F. Borondo, J. Chem. Phys. 129 (2008) 164316.
[13] E.J. Heller, Chaos and Quantum Physics, in: M. Giannoni, A. Voros, J. Zinn-Justin (Eds.), Elsevier, Amsterdam, 1991.
[14] R. Prosmiti, C. Cunha, P. Villarreal, G. Delgado-Barrio, J. Chem. Phys. 116 (2002) 9249.
[15] G. Birkhoff, Dynamical Systems, American Mathematical Society, New York, 1927;
H.R. Dullin, A. Wittek, J. Phys. A: Math. Gen. 28 (1995) 7157.
[16] E. Hairer, S.P. Norsett, G. Wanner, Solving Ordinary Differential Equations. I. Nonstiff Problems, Springer Ser. Comput. Math., Springer-Verlag, 1993.
[17] M. Hénon, Ann. Astrophys. 28 (1965) 992.
[18] E.J. Doedel, R.C. Paffenroth, A.R. Champneys, T.F. Fairgrieve, Yu.A. Kuznetsov, B. Sandstede, X. Wang, AUTO 2000: Continuation and bifurcation software for ordinary differential equations (with HomCont), Technical Report, Caltech, 2001;
F.J. Muñoz-Almaraz, E. Freire, J. Galán, E. Doedel, A. Vanderbauwhede, Physica D 181 (2003) 1.
[19] R. Barrio, F. Blesa, Chaos Solitons Fractals 41 (2009) 560.
[20] Cl. Froeschlé, R. Gonczi, E. Lega, Planet. Space Sci. 45 (1997) 881;
R. Barrio, Int. J. Bifur. Chaos 16 (2006) 2777;
R. Barrio, W. Borczyk, S. Breiter, Chaos Solitons Fractals 40 (2009) 1697.